Modelling of a High-Temperature Superconductor HVDC Cable Under Transient Conditions

Pavan Chaganti, Weijia Yuan, Senior Member, IEEE, Min Zhang, Member, IEEE, Lie Xu, Senior Member, IEEE, Eoin Hodge, and John Fitzgerald

***Abstract* —The carbon neutrality goal of achieving net-zero by 2050 has sparked significant interest in offshore wind farms. With the offshore wind farms installed > 100 km away from the seashore, underground power transmission infrastructure is a necessity. Considering the power cable length and low net effective losses, a high-voltage direct-current (HVDC) system is chosen for this study. Also being lossless in DC operation, the HVDC cables are considered to be made out of high-temperature superconductor (HTS) material. But, unlike copper/aluminium, HTS material has a sharp transient behaviour as a function of the operating current, temperature and field. Thus, under transient conditions, as the fault current ramps up, this can lead to an increase in the HTS operating temperature, causing either degradation or permanent damage to the HVDC cable. In this paper, an HTS HVDC cable model has been developed in MATLAB/Simscape coupling both electrical and thermal models. For this study, a 100 km long coaxial 100 kV/1 GW DC HTS power cable is considered and modelled both as a lumped element and distributed element model with 100 elements to compare and evaluate the cable parameters along the length. The parameters include temperature distribution, resistance, critical current, and losses at different spots throughout the length of the cable. To simulate the transient condition, a line-to-ground (LG) fault is considered and the current distribution between the copper former and HTS tapes is studied. Using this cable model, the maximum temperature of the HTS and coolant both in the superconducting state and transient state are evaluated and presented. In comparison to the distributed model, the lumped model displayed different thermal and electrical values.**

***Index Terms*— High-temperature superconductor, HVDC, LG fault, and offshore wind farm (OWF).**

I. Introduction

The environmental concern has shifted energy generation from non-renewable to renewable energy to reduce carbon emissions to net zero. Energy generation especially from offshore wind farms (OWF) has increased. The present global generation from offshore wind farms is around 40 GW and is projected to be 640 GW by 2050. Nowadays offshore wind farms are constructed upto 100 km away from the shore. DC cables are more suitable to transfer power than AC cables due to the low power loss and no limitation on the length of the cable [1], [2].

With the increased number of OWFs, the power rating of the HVDC system is in the GW range. To reduce transmission losses, extra or ultra-high voltage direct current (EHVDC or UHVDC) cables were developed to transfer high power where the voltage is above 500 kV. This increases the footprint of the offshore platforms makes them uneconomic. Superconductors have the advantage of high current density and coolants like LN_2 are used for both cooling and insulation purposes. Superconductors have advantages such as their low losses, no electromagnetic interference, and small footprint. All these advantages make the HTS suitable for OWF energy transmission applications. Over the last two decades, several projects using HTS cables were tested and operated for the full application of HTS cables in the power grid [3]–[5]. The bulk application of the HTS in the power grid is limited by the factors such as the reliability of the cooling system, the cost of the HTS and overall complexity [6]. Prior to the installation of long-distance cable experiments or lab prototypes, modelling and simulation work is required to predict cable behaviour. Furthermore, modelling the HTS power cable is necessary for enhancing cable performance and design.

Recently various numerical models have been developed based on a time-dependent thermal and electromagnetic model in MATLAB [7], [8], ANSYS [9], PSCAD [10], [11], and COMSOL [12]. The proposed numerical models employ finite element analysis (FEA), finite-difference time-domain (FDTD) analysis and time-frequency domain reflectometry (TFDR) mainly for calculating local electromagnetic behaviours of the cable i.e. local hot spot, AC losses. A recent cable model developed in A1 investigates the HTS model with single-element and single-layer cable model by considering the LN_2 temperature always at 77 K in steady and transient conditions [13]. For the long-distance and fault scenario condition simulations, a circuit model considering LN_2 layer temperature is needed.

In this work, the long-distance cable electrical-thermal model by volume element method is developed in MATLAB/Simscape by dividing the cable into 100 1 km long sections connected in series by considering the copper former and Coolant layers along with the HTS tapes in each section. This model's advantage is its ability to realistically show the thermal model at various cable sites by including several cryocoolers and joint resistance along the length of the cable. When simulating the HTS cable under transient conditions, we concentrated on the

This work was supported through the collaboration project between SuperNode and the Offshore Renewable Energy Catapult (OREC) as part of the Research Programme of the OREC Electrical Infrastructure Research Hub. (Corresponding author: Pavan Chaganti and Weijia Yuan)

Pavan Chaganti, Weijia Yuan, Min Zhang, and Lie Xu are with the Department of Electronic and Electrical Engineering, University of Strathclyde, Glasgow G1 1RD, U.K. (e-mail: lakshmana.chaganti@strath.ac.uk; weijia.yuan@strath.ac.uk).

Eoin Hodge and John Fitzgerald are with the SuperNode, Dublin D22 HC81, Ireland.

This is a peer reviewed, accepted author manuscript of the following research article: Chaganti, P., Yuan, W., Zhang, M., Xu, L., Hodge, E., & Fitzgerald, J. (2023). Modelling of a high-temperature superconductor HVDC cable under transient conditions. *IEEE Transactions on Applied Superconductivity*, 33(5), [5400805]. https://doi.org/10.1109/tasc.2023.3251948

lumped and distributed LC model as well as element size simulation models.

II. Simulation Methodology

The resistance of the superconductor is calculated using the Ic, temperature, and n values from the experimental results mentioned in the reference [14].

The E-J characteristic of the HTS tape was used to calculate the resistance of HTS [15]:

$$R_{hts} = \frac{E_0}{J_c}\left(\frac{J}{J_c}\right)^{n-1}\frac{l}{A} \quad (1)$$

E_0 = electric-field criterion of 1×10^{-4} V/m, J_c = critical current density and J = current density. The n value gives the dependency of the V on the electric current in terms of transition I_c and l is the length of the tape.

The resistance of the Copper layer is dependent on the temperature and geometrical structure. The resistance of the copper stabilizer (R_{cu}) and the copper former (R_f) is calculated for a temperature range of 65 to 600 K using equation 2 [10].

$$R_{cu} = R_f = (0.0635T_i - 2.4641)10^{-9}\frac{l}{A} \quad (2)$$

Where A is the cross-sectional area of the respective layer.

The resistance of the HTS cable is determined by equation 3

$$R = \frac{R_{cu}R_fR_{hts}}{R_{cu}R_f + R_{hts}R_f + R_{cu}R_{hts}} \quad (3)$$

The key parameters that need to be studied for the transient analysis are temperature, resistance, critical current, and current in the network. The cable parameters used in the simulation of the network model was listed in Table 1. In the cable, each element is divided into four layers along the r direction.

TABLE I
HTS CABLE DETAILS

Layer	Radius (mm)	Parameter	Value
Copper former	*20.5*	*Cable length*	*100 km*
		Joint resistance	*90 nΩ*
HTS tapes	*27*	*Critical current (Ic)*	*13900 A*
PPLP	*37*	*Capacitance (C)*	*0.076 μF/km*
LN_2	*90*	*Inductance (L)*	*1.43 mH/km*

The pressure drop (ΔP) in the cryogenic pipe is calculated by the Darcy-Weisbach equation [16]:

$$\Delta P = \frac{fL\rho v^2}{2D_h} \quad (4)$$

Where f friction factor, D_h- hydraulic diameter of HTS cable and return path, ρ density of LN_2, and v – velocity of LN_2. The condition pressure drop is proportional to the length of the cable only if the mass flow is maintained constant.

The hydraulic diameter is equal to

$$D_h = d_o - d_i \quad (5)$$

d_o, and d_i are the outer and inner diameters of the coolant cross-section, respectively.

The heat load per unit length due to friction losses between the coolant and pipe surface is a product of the volume flow and pressure drop [17]. The friction losses are given as

$$Q_f = \frac{\Delta P}{L}\dot{V} = \frac{\Delta P.m}{L.\rho} \quad (6)$$

The first law of thermodynamics is applied to each layer in the cable. Consecutive equations are used to evaluate the heat fluxes and physical properties between layers in the r and z directions. During the steady state the term $\frac{dT}{dt}$ is assumed as $(T_{final} - T_{initail})$.

For the copper layer,

$$M_{cu}cp_{cu}\frac{dT1}{dt} = (Q_{12} + Q_{1in} - Q_{1out} + Q_{former}) \quad (7)$$

For superconductor layer

$$M_{hts}cp_{hts}\frac{dT2}{dt} = (Q_{hts} - Q_{12} - Q_{23} + Q_{2in} - Q_{2out}) \quad (8)$$

$$cp_{hts} = (2T_2d_{hts}t_{hts} + 2T_2d_{hastelloy}t_{hastelloy} + cp_{cu}d_{cu}t_{cu})w \times l \times n1 \quad (9)$$

Where w is the width of the tape, n1 is the number of tapes, $d_{hts}, d_{hastelloy}, d_{cu}$ are the density of the materials in the HTS tapes and similarly $t_{hts}, t_{hastelloy}, t_{cu}$ are thickness.

For the dielectric layer,

$$M_{pplp}cp_{pplp}\frac{dT3}{dt} = (Q_{23} + Q_{3in} - Q_{3out} - Q_{34} + Q_{pplp}) \quad (10)$$

For the cryogenic coolant layer,

$$M_{ln2}cp_{ln2}\frac{dT4}{dt} = (Q_{34} + Q_{4in} - Q_{4out} + Q_f + Q_o) \quad (11)$$

The losses in the copper, HTS and PPLP are measured as follows

$$Q_{fomer} = i^2_{former}R_f \quad (12)$$

$$Q_{gen} = Q_{hts} + i^2_{hts} * R_{hts} + i^2_{cu}R_{cu} \quad (13)$$

$$Q_{pplp} = 2\pi f\tan(\delta)\varepsilon(10^{-11})\frac{v^2}{2\log(\frac{r_3}{r_2})^2} \quad (14)$$

The Q_{hts} calculated using the Norris equation from reference [18]. The heat through the conduction, convective and radiative in the cable $(Q_{12}, Q_{23}, Q_{34}, Q_{1in}, Q_{1out}, Q_{2in}, Q_{2out}, Q_{3in}, Q_{3out}, Q_{4in}, Q_{4out}, Q_o)$ is calculated as mentioned in reference [7]. Where M and cp are mass in [Kg] and specific heat at constant volume in [J/KgK] with subscript indicates particular layer of the cable.

The flowchart in Fig. 1(a) illustrates the detailed steps from resistor component design to network modelling. The component R was developed in MATLAB/Simscape using the equations mentioned above. Fig. 1(b) shows the HTS HVDC Subsea cable structure.

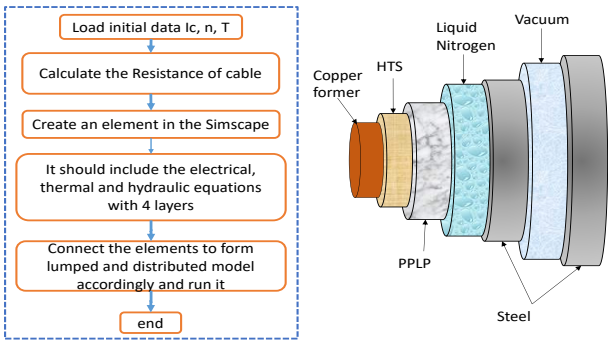

(a) (b)

Fig. 1. (a) Flow chart explains the step-by-step simulation procedure in MATLAB and (b) HTS HVDC Subsea cable structure

The MATLAB simulation model schematic view was shown in Fig. 2. Fig. 2(a) shows the lumped network model of the cable where L, C and R values for 100 km long. Fig. 2(b) shows the lumped L, C with distributed R model and Fig. 2(c) shows the distributed network model where L, C and R values for 1 km long. Each R, L, and C are arranged as a π section. R represents the four layers of the cable. It is assumed that the superconducting tape is a homogeneous medium that describes all of the tape layers. The initial temperature of all the layers in the cable is considered 70 K.

The network model built in MATLAB/Simscape was 100 km long with 100 kV DC and the operating current is 10 kA. A temporary Line to Ground fault at the end of the cable was initiated at time=10 sec in the simulation for a duration of 20 ms. The simulation is carried out by keeping the consistency tolerance=10^{-9} and sample time=10^{-3} sec.

Fig. 3(a) represents the cable structure used in the R component. It consists of copper, HTS, polypropylene laminated paper (PPLP) and liquid nitrogen (LN_2) layers. Fig. 3(b) shows the volume element discretization of the HTS and shows the heat transfer between the layers along the r and z direction. The heat transfer from the outside cable environment through the

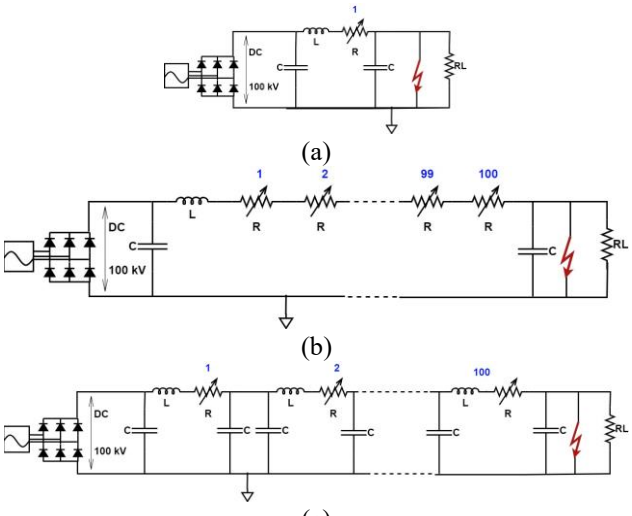

(a)

(b)

(c)

Fig. 2. Simulation circuit schematic view (a) lumped cable model, (b) Lumped L,C and distributed R and (c) Distributed L,C,R cable model with 100 cable blocks.

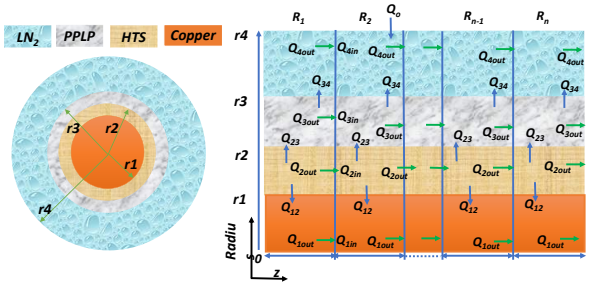

(a) (b)

Fig. 3. (a) Cross-section view and (b) volume element discretization of HTS cable.

vacuum layer is numerically measured, and element discretization is not considered for this layer. For the distributed LC model with 100 components, the computational burden is 4.5 hours, using an Intel(R) Core (TM) i7-7700 CPU @ 3.60 GHz with installed of RAM 32 GB.

III. Results and Discussion

The HTS cable is energised with DC voltage using AC/DC converter circuit which gives an output of 100 kV DC voltage. Under steady-state conditions, the temperature of the superconductor is almost similar along the length of the cable. Under transient conditions, the receiving end of the cable is short-circuited to the ground. The run time for the lumped LC model shown in Fig. 2(a) takes 2 minutes and for distributed LC shown in Figs. 2(b) and 2(c) takes 4.5 hours each.

Fig.4 (a) depicts the temperature of the HTS and copper former. The HTS tapes reach 230.5 K, and the copper former reaches 234.6 K. The resistance of the cable is shown in Fig.4 (b). The resistance of the cable reaches the maximum value of 0.93 Ω. The quench recovery time of the superconductor takes around 227 sec for the lumped model to reach T<Tc (critical temperature (Tc)=87.5 K). During the fault, the current rises to

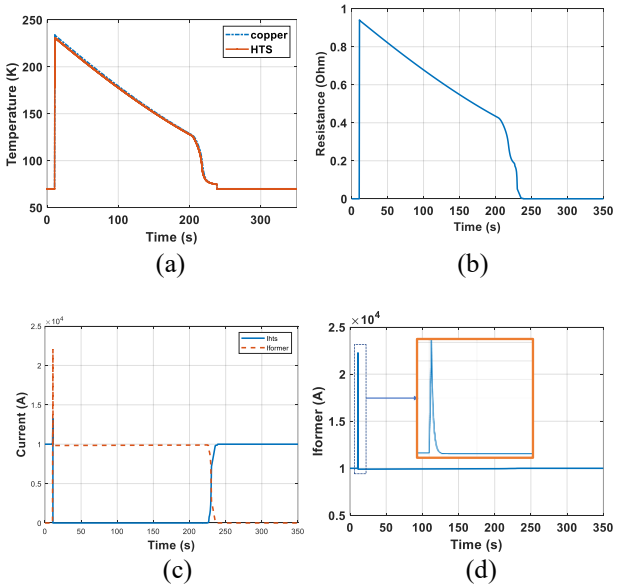

(a) (b)

(c) (d)

Fig. 4. Lumped model single element (a) temperature of HTS and copper former, (b) resistance of the cable, (c) current flow in the HTS and former layers and (d) current flow in the cable.

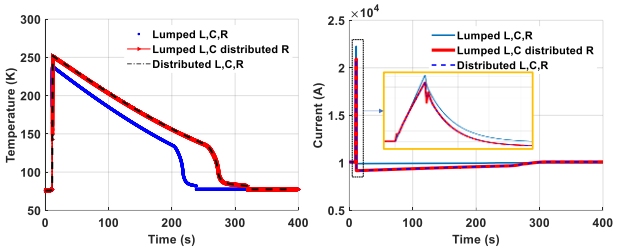

Fig. 5. Distributed elements used are 50 with element size 2 km (a) HTS Temperature and (b) current in the cable.

22 kA, and once the current reaches the critical current value of 13.9 kA, the resistance of the HTS increases with a rise in the temperature, $R_{hts}>R_f$ the current shifts from the HTS to the copper former as shown in Fig. 4(c) and prevents damage to the HTS layers. Fig. 4(d) depicts the current in the cable.

The behaviour of the cable is the same whether it is distributed LC or lumped LC with distributed R, as shown in Fig. 5. This is so because the cable's overall LC values are the same in both scenarios. The distributed model has a higher temperature than the lumped L, C and R model, and its current limiting difference during the fault is about 1 kA.

The HTS temperature and pressure are shown in Fig. 6(a) at various locations throughout the cable's length in a steady state. The LN_2's pressure was kept between 3 and 20 Bar. For pressure higher than 20 Bar it deforms the cable and maintained >3 to prevent the boiling of LN_2. To prevent the quenching of the HTS cable, the temperature of the LN_2 was maintained between 65 and 77 K. Ten cryocoolers were taken into consideration for a 100 km long cable to meet these requirements. Under normal conditions, the cable's pressure drop is 1.5 bar/km. The ac losses are small, the reason for the temperature rise is the heat transfer from the outside environment to LN_2 and friction losses in the hydraulic path. Fig. 6(b) shows the critical current of the cable along the length of the cable. The Ic is 13.9 kA at 70 K, and as the temperature rises, it decreases until it is 12.1 kA at 76.4 K.

Fig. 7 shows the behaviour of the cable going from normal to a quenched state and back to normal condition. The 10 km cable section in fig. 7(a) shows that the initial portion of the cable temperature is a little lower than the final portion. The temperature difference is 6.3 K. Fig. 7(b) displays the temperature of the LN_2 along the length w.r.t time on a 10 km cable section. The maximum temperature reached by the LN_2 is 91.8 K. Due to the heat transfer coefficient, a second peak is seen at 200 seconds. The reference [19] shows that the h value changes

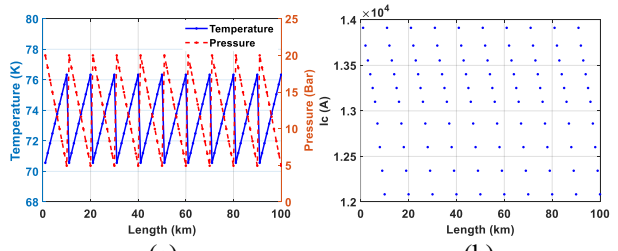

Fig. 6. Cable with 100 elements with element size 1 km (a) Temperature and pressure of LN_2 for m=4 kg/s and (b) critical current of the cable.

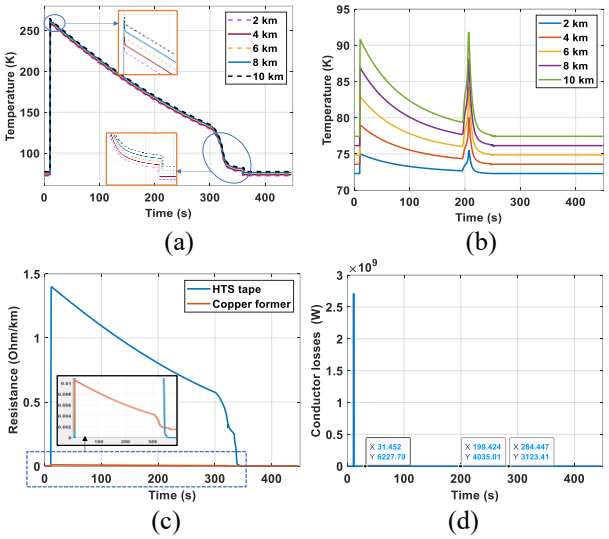

Fig. 7. With 100 elements 1 km long each (a) HTS temperature, (b) Temperature of LN_2 after fault initiates, (c) Resistance of HTS and copper former and (d) cable losses

dramatically when the temperature differential between the HTS and LN_2 is between 5 and 50 K. After the fault occurs, the LN_2 temperature is below the boiling point, or 77 K, for a distance of 0-2 km. Due to joule heating, the LN_2 begins to boil along the remaining 2–10 km of cable.

Fig. 7(c) shows the resistance of the superconductor layer and copper former. Under normal conditions, the resistance of the HTS layer is almost zero. But at the instant of the fault, the R_{hts} reaches above 1.4 Ω/km. During the normal condition the $R_{hts}<< R_f$ and during the transient, there is a sharp rise in the $R_{hts}>>R_f$. During the steady state, the losses in HTS and former layers are 0.175 W/km. Whereas during a fault condition, it reaches 2.7×10^4 W/m as depicted in Fig. 7(d).

During the transient condition, the temperature difference between lumped model and distributed model with 50 elements is around 14 K. Whereas the difference between the distributed model with 50 and 100 elements is less than 7 K as shown in Fig. 8(a). The temperature deviation is not much and other characteristics are similar, so the distribution LC model with 100 elements is sufficient for the cable model to study the thermal behaviour along the length of the cable. It takes 55 seconds longer to reach the pre-fault condition for this 7 K temperature difference. In the quenched state condition, the former temperature is higher than HTS in all scenarios.

The superconductor quench recovery along the length of the cable changes. The cable's initial part which is near the voltage

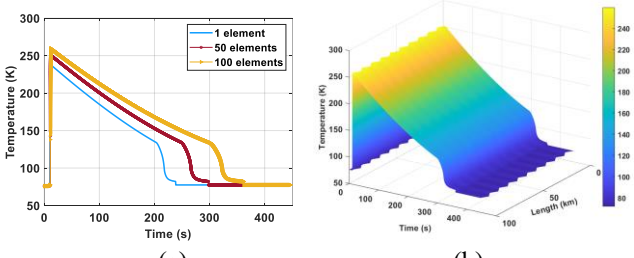

Fig. 8. Thermal behaviour of the superconductor of 100 km long (a) element size comparison and (b) 3D view of HTS temperature.

source recovers from the quench faster than the end part near the fault. As this is due to the low temperature of the cable at the initial section and the other was due to LN_2 first passing through this section and cooling it down. For every 10 km cable section, the initial part of the cable recovers from the quench and operates as pre-fault condition 6 sec ahead of the endpoint of the 10 km cable section as shown in Fig. 8(b). The cable thermal behaviour repeats every 10 km under stable and transient conditions since the model uses 10 cryocoolers.

IV. Conclusion

To interconnect the offshore and onshore grids, we developed a simplified distributed model of a multilayer HTS power cable for a long-distance HVDC system. The simulation results show, the temperature, resistance and losses and current distribution in normal and in transient conditions along the length of the cable. No difference exists in the thermal properties whether the LC is distributed or lumped. We can use either lumped or distributed L and C with distributed R in the model. The superconductor quenches and current flows through the copper former for 6 minutes after the temporary LG fault. After the fault is cleared, the current drops instantly below the operating current, and the temperature begins to decay slowly and reaches below Tc then it back to a superconducting state. Multiple cryocoolers are required rather than a single cryocooler to prevent LN_2 from boiling for such long-distance power transmission. The quantity of distributed R elements required was demonstrated. Investigation results indicate that the cable cannot be permanently damaged in this fault condition.

References

[1] D. Elliott *et al.*, "A Comparison of AC and HVDC Options for the Connection of Offshore Wind Generation in Great Britain," *IEEE Trans. Power Deliv.*, vol. 31, no. 2, pp. 798–809, 2016, doi: 10.1109/TPWRD.2015.2453233.

[2] V. E. Sytnikov *et al.*, "HTS DC Cable line project: On-Going activities in Russia," *IEEE Trans. Appl. Supercond.*, vol. 23, no. 3, pp. 2–5, 2013, doi: 10.1109/TASC.2013.2245280.

[3] B. Yang, J. Kang, S. Lee, C. Choi, and Y. Moon, "Qualification Test of a 80 kV 500 MW HTS DC Cable for Applying into Real Grid," *IEEE Trans. Appl. Supercond.*, vol. 25, no. 3, 2015, doi: 10.1109/TASC.2015.2396683.

[4] M. Stemmle, F. Merschel, M. Noe, and A. Hobl, "AmpaCity — Installation of advanced superconducting 10 kV system in city center replaces conventional 110 kV cables," in *2013 IEEE International Conference on Applied Superconductivity and Electromagnetic Devices*, 2013, pp. 323–326, doi: 10.1109/ASEMD.2013.6780785.

[5] M. Nassi, N. Kelley, P. Ladié, P. Corsaro, G. Coletta, and D. Von Dollen, "Qualification results of a 50 m-115 kV warm dielectric cable system," *IEEE Trans. Appl. Supercond.*, vol. 11, no. 1 II, pp. 2355–2358, 2001, doi: 10.1109/77.920334.

[6] D. I. Doukas, Z. D. Blatsi, A. N. Milioudis, D. P. Labridis, L. Harnefors, and G. Velotto, "Damping of electromagnetic transients in a superconducting VSC transmission system," in *2015 IEEE Eindhoven PowerTech*, 2015, pp. 1–6.

[7] D. I. Doukas, A. I. Chrysochos, T. A. Papadopoulos, D. P. Labridis, L. Harnefors, and G. Velotto, "Coupled Electro-Thermal Transient Analysis of Superconducting DC Transmission Systems Using FDTD and VEM Modeling," *IEEE Trans. Appl. Supercond.*, vol. 27, no. 8, 2017, doi: 10.1109/TASC.2017.2749500.

[8] R. Su *et al.*, "Numerical Model of HTS Cable and Its Electric-Thermal Properties," *IEEE Trans. Appl. Supercond.*, vol. 29, no. 5, 2019, doi: 10.1109/TASC.2019.2901874.

[9] Z. Zhou *et al.*, "Magnetic-thermal coupling analysis of the cold dielectric high temperature superconducting cable," *IEEE Trans. Appl. Supercond.*, vol. 23, no. 3, p. 5400404, 2012.

[10] T. Nguyen *et al.*, "A Simplified Model of Coaxial, Multilayer High-Temperature Superconducting Power Cables with Cu Formers for Transient Studies," 2019.

[11] W. Xiang *et al.*, "DC Fault Study of a Point-to-Point HVDC System Integrating Offshore Wind Farm Using High-Temperature Superconductor DC Cables," *IEEE Trans. ENERGY Convers.*, vol. 37, no. 1, pp. 377–388, 2022, doi: 10.1109/TEC.2021.3094308.

[12] W. T. B. De Sousa, D. Kottonau, and M. Noe, "Transient Simulation and Recovery Time of a Three-Phase Concentric HTS Cable," *IEEE Trans. Appl. Supercond.*, vol. 29, no. 5, 2019, doi: 10.1109/TASC.2019.2900937.

[13] Strickland, N. M., C. Hoffmann, and S. C. Wimbush. "A 1 kA-class cryogen-free critical current characterization system for superconducting coated conductors." Review of Scientific Instruments 85, no. 11 (2014): 113907.

[14] N. Endo, Y. Shinozaki, Y. Nagasaki, D. Miyagi, and M. Tsuda, "Configuration method of tri-axial ReBCO cable suitable for long distance power transmission," *IEEE Trans. Appl. Supercond.*, vol. 29, no. 5, 2019, doi: 10.1109/TASC.2019.2904546.

[15] Z. Q. Zuo, W. B. Jiang, Z. G. Yu, and Y. H. Huang, "Liquid nitrogen flow in helically corrugated pipes with insertion of high-temperature superconducting power transmission cables," *Int. J. Heat Mass Transf.*, vol. 140, pp. 88–99, 2019, doi: 10.1016/j.ijheatmasstransfer.2019.05.078.

[16] B. Zajaczkowski, A. J. M. Giesbers, M. Holtrust, E. Haenen, and R. Den Heijer, "Feasibility of inline cooling in long distance HTS power line," *Cryogenics (Guildf).*, vol. 51, no. 4, pp. 180–186, 2011, doi: 10.1016/j.cryogenics.2011.01.007.

[17] Y. Ivanov *et al.*, "Current Imbalance and AC Losses of Long-Distance DC HTS Cable," *IEEE Trans. Appl. Supercond.*, vol. 26, no. 7, pp. 3–6, 2016, doi: 10.1109/TASC.2016.2577600.

[18] T. Jin, J. Hong, H. Zheng, K. Tang, and Z. Gan, "Measurement of boiling heat transfer coefficient in liquid nitrogen bath by inverse heat conduction method," *J. Zhejiang Univ. A*, vol. 10, pp. 691–696, 2009.